Microbiome

RESEARCH

Open Access

CHIKV infection drives shifts in the gastrointestinal microbiome and metabolites in rhesus monkeys

Hongyu Chen[1†], Jiandong Shi[1†], Cong Tang[1†], Jingwen Xu[1†], Bai Li[1], Junbin Wang[1], Yanan Zhou[1], Yun Yang[1], Hao Yang[1], Qing Huang[1], Wenhai Yu[1], Haixuan Wang[1], Daoju Wu[1], Yunzhang Hu[1*], Hongning Zhou[2*], Qingming Sun[1,3,4*] and Shuaiyao Lu[1,3,4*]

Abstract

Background Many studies have demonstrated the association between intestinal microbiota and joint diseases. The "gut-joint axis" also has potential roles in chikungunya virus (CHIKV) infection. Pro-inflammatory arthritis after CHIKV infection might disrupt host homeostasis and lead to dysbacteriosis. This study investigated the characteristics of fecal and gut microbiota, intestinal metabolites, and the changes in gene regulation of intestinal tissues after CHIKV infection using multi-omics analysis to explore the involvement of gut microbiota in the pathogenesis of CHIKV infection.

Results CHIKV infection increases the systemic burden of inflammation in the GI system of infected animals. Moreover, infection-induced alterations in GI microbiota and metabolites may be indirectly involved in the modulation of GI and bone inflammation after CHIKV infection, including the modulation of inflammasomes and interleukin-17 inflammatory cytokine levels.

Conclusion Our results suggest that the GI tract and its microbes are involved in the modulation of CHIKV infection, which could serve as an indicator for the adjuvant treatment of CHIKV infection.

Keywords CHIKV, Gut microbiota, Pro-inflammatory arthritis, NHP model, Integrative analysis

[†]Hongyu Chen and Jiandong Shi, Cong Tang and Jingwen Xu contributed equally to this work.

*Correspondence:
Yunzhang Hu
huyunzhangym@126.com
Hongning Zhou
zhouhn66@163.com
Qingming Sun
qsun@imbcams.com.cn
Shuaiyao Lu
lushuaiyao-km@163.com
[1] Institute of Medical Biology, Chinese Academy of Medical Sciences and Peking Union Medical College (IMBCAMS&PUMC), 935 Jiaoling Road, Kunming, Yunnan 650118, China
[2] Yunnan Provincial Key Laboratory of Insect-Borne Infectious Diseases Control & Yunan International Joint Laboratory of Tropical Infectious Diseases of Yunnan Institute of Parasitic Diseases, Puer, Yunnan 665000, China
[3] Key Laboratory of Pathogen Infection Prevention and Control (Peking Union Medical College), Ministry of Education, Beijing, China
[4] State Key Laboratory of Respiratory Health and Multimorbidity, Beijing, China

Introduction

Chikungunya virus (CHIKV) belongs to the *Alphavirus* genus within the family Togaviridae and is an enveloped, icosahedral, and RNA arthropod-borne virus [1]. It (CHIKV) is sensitive to dryness and high temperatures (> 58 °C) [2], and the area where the virus is present spreads with the distribution expansion of mosquito vectors (*Aedes aegypti* and *Aedes albopictus*) [3]. Moreover, it circulates in a human-mosquito-human transmission cycle. Three main lineages with different genetic and antigenic characteristics have been identified: the African (West African and East/central South African), Indian Ocean, and Asian lineages [4].

CHIKV has a diameter of approximately 70 nm [5]. It possesses a positive-sense RNA genome of 11.5 kb that encodes four non-structural proteins (nsPs), including methyltransferase (nsP1), protease and helicase (nsP2), ADP-ribohydrolase (nsP3), and RNA-dependent RNA polymerase (nsP4), as well as three structural proteins (envelope glycoproteins, E1, and E2) and two small peptides (E3 and 6 K) [6]. The main targets of CHIKV are synovial macrophages, muscle cells, and synovial fibroblasts. CHIKV infection leads to chikungunya fever, characterized by symptoms such as fever (body temperature > 38.9 °C), muscle stiffness, and debilitating joint diseases [7]. While CHIKV infection is non-lethal (mortality rate < 0.5%) [8], its strong infectivity and the high number of infected individuals have severely affected their quality of life and social development [9]. Since 1950, more than one million people have been affected by CHIKV infection, primarily in Southeast Asian and European countries, and the infection continues to spread [10].

As the "second genome" of animals, the complex symbiotic microbiota in the gastrointestinal (GI) tract plays a crucial role in host nutrition absorption and immunity [11]. It is considered an "organ" with endocrine and immune functions, which are directly related to viral infections [12], regulation of cellular inflammation [13], and immune cell maturation [14], such as promoting the development and maturation of Th1, Th2, Th17, and regulatory T cells (Tregs) [15].

Inflammatory cytokine storms stimulate bone degradation and joint damage, which are the key drivers of arthritis [16]. However, the mechanisms underlying CHIKV-induced arthritis remain unclear. The pro-inflammatory arthritis observed in CHIKV-infected patients is highly similar to rheumatoid arthritis (RA), both in terms of pathology and gene expression, and is characterized by pro-inflammatory cytokine- and chemokine-driven inflammatory responses [17]. RA has genetic components, with a heritability of approximately 60%. In particular, the "shared epitope" of *HLA-DRB1* alleles has been reported to be associated with the pathogenesis of RA [18]. Moreover, growing evidence suggests that dysbiosis of the gut microbiota plays a significant role in the immune regulation defects in RA. Hager et al. found that gut microbial dysbiosis was observed in most patients with RA, and supplementation with a high-fiber diet or short-chain fatty acids (SCFAs) increased the number of Tregs and the Th1/Th17 ratio to enhance the anti-inflammatory process, reduce arthritis, and inhibit bone loss [19]. Furthermore, many studies have demonstrated the association of intestinal microflora with joint diseases such as osteoarthritis, RA, and secondary arthritis, suggesting a "gut-joint axis" [20, 21]. Microbial metabolites (microbe-associated molecules) enter the systemic circulation through the gut barrier and trigger pro-inflammatory responses in resident immune cells, leading to joint inflammation [22]. Therefore, although CHIKV is not an enteric virus, we hypothesized that CHIKV infection may lead to systemic inflammation and disrupt host homeostasis, resulting in dysbacteriosis and altered metabolite profiles that affect immunoregulatory processes and promote (or alleviate) joint inflammation. Furthermore, the intestinal tract may also be involved in synergistic immunity after CHIKV infection. To test this hypothesis, This study investigated the characteristics of fecal and gut microbiota (composition, structure, and metabolism) and the changes in gene regulation of intestinal tissues at the transcriptional level after CHIKV infection using a multi-omics analysis based on an established non-human primate (NHP) model to explore the involvement of gut microbiota in the pathogenesis of CHIKV infection.

CHIKV has become a significant public health burden. However, there are currently no officially approved drugs for its prevention or treatment, the findings of this study can facilitate our understanding of the role of gut microbiota in viral infections and provide a theoretical basis for diverse treatment strategies for chikungunya fever.

Materials and methods

Statements of animal ethics and biosafety

According to the classification of CHIKV pathogenicity, all experiments involving live CHIKV and animal challenges were conducted in an animal biosafety level 3 laboratory. All animal procedures were approved by the Institutional Animal Care and Use Committee of the Institute of Medical Biology, Chinese Academy of Medical Science (approval number: DWSP20210006).

CHIKV strains and animal experimental procedures

Six rhesus monkeys were randomized into a negative control (NC) group (treatment with phosphate-buffered saline; NC1, female, 12 years old; NC2, male, 9 years old; NC3, male, 12 years old) and a challenge group (C1, female, 14 years old; C2, male, 8 years old; C3, male,

7 years old). Each animal was housed separately and fed commercial monkey chow and fruit. Before CHIKV challenge all rhesus monkeys received background testing to ensure that they were not infected with CHIKV and free of basic diseases such as arthritis and digestive system diseases. The animals were challenged with CHIKV at a dose of 2×10^7 PFU through leg muscle injections, and fresh feces were collected daily for seven consecutive days. At 7 dpi, all animals were anesthetized and dissected. The small and large intestine contents were carefully extracted and separated into two parts for microbial metagenome and untargeted metabolomics analyses. All experiments were performed on a super clean workbench to prevent contamination. Tissues (small and large intestine, and blood) were harvested for histological and transcriptomic analyses. Further details are presented in Fig. 1A.

Determination of viral load in intestinal contents and other tissues

The Direct-zol RNA Miniprep Extraction Kit (Zymo Research, Catalog no. R2052) was used for viral RNA extraction from tissues according to the manufacturer's instructions. Viral RNA (E1 gene) was used for the standard curve to quantify the genomic RNA of CHIKV in each tissue, blood, or fecal content by calculating the copy number. The primers included CHIKV E1F (CTC ATACCGCATCCGCATCAG), E1R (ACATTGGCCCCA CAATGAATTTG), and CHIKV E1 Probe (FAM-TCC TTAACTGTGACGGCATGGTCGCC-BHQ1).

Histopathologic analysis

Tissue samples (except ankles) were fixed in 10% neutral-buffered formalin for at least 10 days after collection. Subsequently, all tissues underwent paraffin sectioning and were stained with hematoxylin and eosin (H&E) for histopathological analysis. The stained sections were scanned using 3D HISTECH(Hungary). Pathological evaluations were statistically analyzed after scoring by experienced pathologists based on histological lesions (0, absent; 1, slight; 2, mild; 3, moderate; and 4, severe) and inflammatory cell infiltration (0, absent; 1, slight; 2, mild; 3, moderate; and 4, severe).

Immunofluorescence analysis

Tissue samples were embedded in paraffin, cut into 3-μm sections, and incubated with primary antibodies anti-ZO-1 (ThermoFisher, Catalog no. 33–9100; 1:100), anti-EpCAM (Abcam, Catalog no. ab282457; 1:100), anti-CD4 (Abcam, Catalog no. ab133616; 1:5000), and CD68 (Catalog no. GB113150; 1:500). Following the addition of the corresponding fluorescent-conjugated secondary antibodies, the sections were counterstained with DAPI and scanned on the 3D HISTECH system (3DHISTECH). Positively-stained cells on each slide were identified using the artificial intelligence image analysis software, Aipathwell (Service Bio). The staining index on each slide was calculated as the percentage of positive cells over the total number of cells and plotted using GraphPad Prism software (version 8.0).

Alcian blue and periodic acid–Schiff staining

GI fragment tissues were embedded in paraffin, cut into 3-μm sections, and stained with Alcian blue and Periodic Acid-Schiff (AB-PAS) staining kit (Catalog no. G1049, Solar Bio) according to the manufacturer's instructions. The stained slides were scanned using a 3D HISTECH system, and goblet cells on each slide were counted as previously described [12]. The slides were equally divided into four parts, in which five crypts were randomly selected to count the goblet cells. Only goblet cells ≥ 150 μm from the surface epithelium of the crypts (longitudinally cut) were counted. The significance of the differences was calculated using Welch's *t* test and plotted using GraphPad Prism software (version 8.0).

(See figure on next page.)

Fig. 1 Histopathological analysis of the GI tissues in rhesus monkeys challenged with CHIKV. **A** Six rhesus monkeys were randomized into a negative control group (NC; treatment with phosphate-buffered saline) and a challenge group. The animals were challenged with CHIKV at a dose of 2×10^7 PFU through leg muscle injections. Fresh fecal and blood samples were collected daily for seven consecutive days. On day 7, all animals were euthanized and dissected for the collection of GI contents and tissues, followed by the evaluation of viral load, pathological histology, transcriptomics, 16S rRNA sequencing, microbial metagenomics, and metabolomics. This figure was prepared using the online software Figdraw (Copyright No. ATTTWb24b7). **B** Viral genomic RNA was detected in the tissues and feces of CHIKV-infected monkeys. At 7 dpi, the animals were euthanized and dissected. Blood, GI tissues, and GI contents/feces were collected for analysis of viral RNA via qRT-PCR as described in the Materials and Methods section. **C** Severity index of histopathology of the indicated tissues. The evaluation of the severity index is described in the Materials and Methods section. *(Welch's t test; *$P<0.05$, **$P<0.01$, ***$P<0.005$, ****$P<0.001$). **D** Left, mucosal barrier integrity of the GI tract was evaluated using AB-PAS staining as described in the "Materials and methods" section. Compared with the NC group, a significant difference in goblet cell count in the GI tissues of variant-infected animals was indicated by Welch's t test and plotted using GraphPad Prism 8.0. *(*$P<0$ .05, **$P<0.01$, ***$P<0.005$, ****$P<0.001$). Right, representative images (Supplemental Figure S1B); CHIKV-1, infected monkey No.1; CHIKV-3, infected monkey No. 3

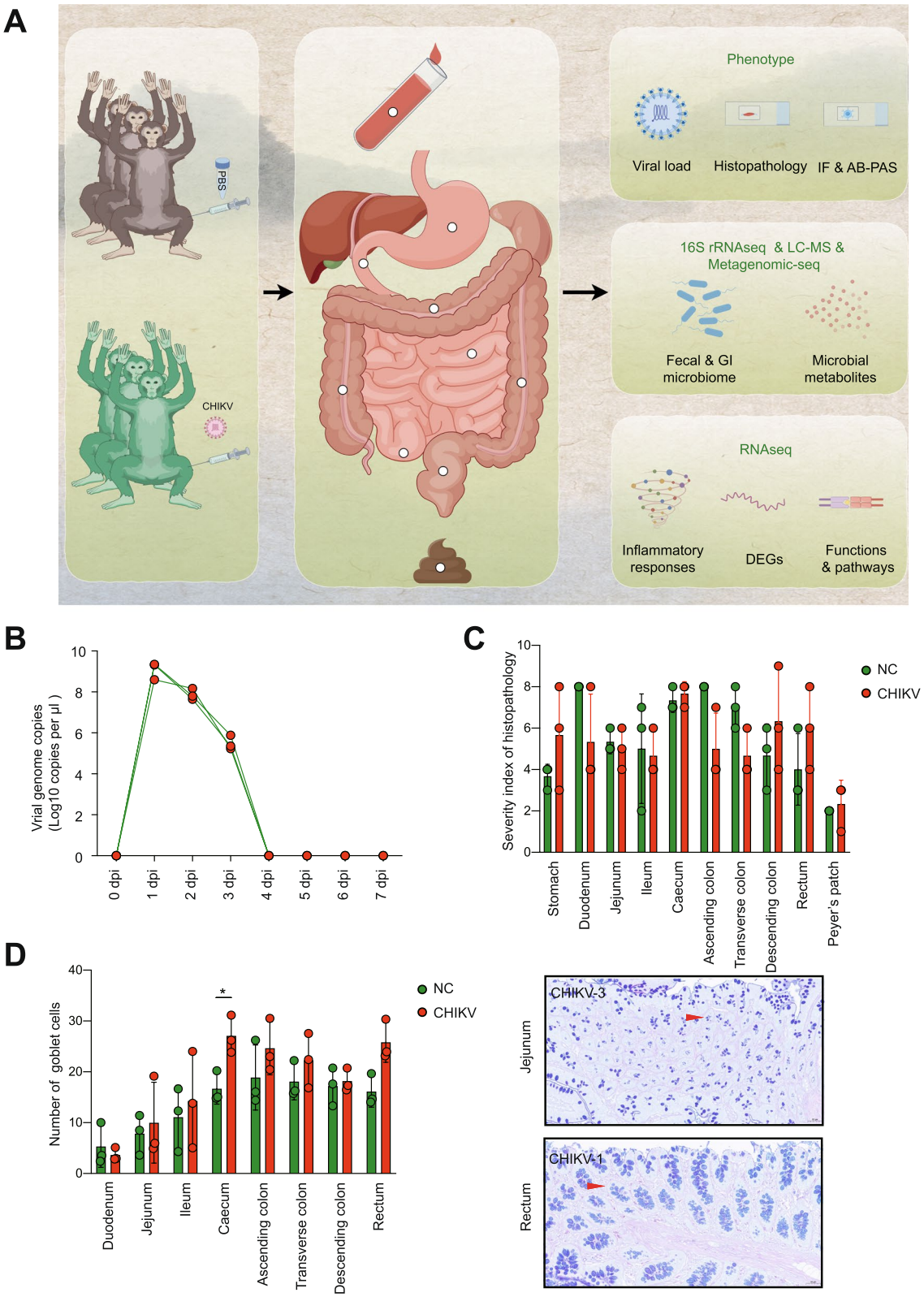

Fig. 1 (See legend on previous page.)

16 s rRNA sequencing regarding the dynamic changes in microbial communities in feces after CHIKV challenge

Fecal samples were collected directly using a DNA/RNA Shield™ Lysis Tube (ZymoBIOMICSTM, Catalog no. R1103-50) to inactivate the virus. Accordingly, fecal microbial DNA was extracted using a DNA Miniprep Kit (ZymoBIOMICSTM, Catalog no. D4300), according to the manufacturer's instructions. DNA quality and concentration were assayed using agarose gel electrophoresis and a NanoDrop ND2000 spectrophotometer (Thermo Scientific Inc., USA). Fecal bacterial 16S rRNA genes (V3–V4) were amplified with primer 338F-806R (5′-ACTCCTACGGGAGGCAGCAG-3′; 5′-GGACTACHVGGGTWTCTAAT-3′) using ABI GeneAmp® 9700 PCR thermocycler (ABI, CA, USA) with the following PCR reaction mixtures: 10 μl 2×Phanta Master Mix, 0.8 μl forward primer (5 μM), 0.8 μl reverse primer (5 μM), 10 ng of template DNA, and ddH2O to a final volume of 20 μL. The PCR conditions were as follows: initial denaturation at 95 ℃ for 3 min, followed by 30 cycles of denaturation at 95 ℃ for 30 s, annealing at 55 ℃ for 30 s, extension at 72 ℃ for 45 s, single extension at 72 ℃ for 10 min, and cooling at 10℃. All samples were amplified in triplicate to meet technical repetition and were quantified using Quantus™ Fluorometer (Promega, USA) after purification with 2% agarose gel. After purification, sequencing libraries of the PCR products were generated using a NEXTFLEX Rapid DNA-Seq Kit (Catalog no. NOVA-5144, Bioo Scientific, Austin, TX, USA) in the following procedures: (i). Ligation of the adaptor, (ii) removal of the splice self-attachment fragment using magnetic bead screening, (iii) enrichment of the library template using PCR amplification, and (iv) PCR product recovery using magnetic beads to obtain the final library and sequencing on Illumina PE300 with assistance from Majorbio Bio-Pharm Technology Co., Ltd. (Shanghai, China).

Following demultiplexing, the raw data were quality-filtered using FASTQ (https://github.com/OpenGene/fastp, version 0.20.0) and merged using FLASH (http://www.cbcb.umd.edu/software/flash, version 1.2.11). Sequencing reads pairing, quality filtering, and chimera removal were conducted using DADA2 (QIIME2 pipeline [version 2022.11]) to obtain a feature table, that is, amplicon sequence variants (ASVs). The number of sequences in each sample was normalized to the minimum number of sequences to eliminate the effect of sequencing depth. To increase the accuracy of the microbial annotation, a 16S rRNA 99% packet (V138) from the SILVA database (https://www.arb-silva.de/download/archive/qiime) was used for classifier self-training (Naive-bayes) according to our primer sequences. Subsequently, ASVs were assigned taxonomically using a self-training classifier. Mothur v1.40.5 (http://www.mothur.org/wiki/Calculators, version 1.40.5) was used for dilution curve plotting and alpha diversity calculation for the ASVs. The Wilcoxon rank-sum test was used to analyze the differences in alpha diversity and abundance between the two groups. Beta diversity was assessed using principal coordinate analysis (PCoA) via the Vegan v2.5–3 package. Moreover, cluster significance was determined using PERMANOVA (permutational analysis of variance). Matrix correlations were assessed using the Pheatmap package (v1.0.12) in R.

Compositional and functional analysis of intestinal contents via metagenomic sequencing

Following the manufacturer's instructions, 0.5 g of the intestinal contents were used to extract total DNA using a PF Mag-Bind Stool DNA Kit (Omega Bio-tek, Norcross, GA, USA). The DNA quality (concentration and purity) was assessed using 1% agarose gel electrophoresis and a NanoDrop ND2000 spectrophotometer (Thermo Scientific Inc., USA). For paired-end library construction, DNA extracts were fragmented into an average size of 400 bp and constructed using NEXTFLEX Rapid DNA-Seq (BioScientific, Austin, TX, USA). Majorbio Bio-Pharm Technology Co., Ltd. (Shanghai, China) performed paired-end sequencing on an Illumina NovaSeq 6000 (Illumina Inc., San Diego, CA, USA) using the NovaSeq 6000 S4 Reagent Kit. Raw data processing was performed using FASTQ (trimmed of adaptors and low-quality reads [length < 50 bp, quality value < 20, or having N bases] were removed). The host genome was removed using the BWA (http://bio-bwa.sourceforge.net, version 0.7.17). Quality-filtered data were assembled using Multiple_MEGAHIT (https://github.com/voutcn/megahit, version 1.1.2), and contigs with lengths > 300 bp were retained. Prodigal and CD-HIT (http://weizhongli-lab.org/cd-hit/, version 4.7) were used for open reading frames prediction and non-redundant gene sit construction (90% sequence identity, 90% coverage), respectively. High-quality reads from each sample were matched to a non-redundant gene set (95% identity) to calculate gene abundance using SOAPaligner (https://github.com/ShujiaHuang/SOAPaligner, version soap2.21release). DIAMOND (http://ab.inf.uni-tuebingen.de/software/diamond/, version 2.0.13) was used to align the non-redundant genes (*e*-value cutoff of 1×10^{-5}, best-hit) with the NCBI NR database for microbial annotation, and gene function (COG, KEGG, VFDB, and CAZy) in each database.

Non-targeted metabolomics of intestinal contents via LC–MS

In a 2-ml centrifuge tube, 100 mg of the sample was added and ground with 6 mm grinding beads for 6 min (-10 °C, 50 Hz). Metabolites in the intestinal contents

were extracted using a methanol:water solution (4:1) containing 0.02 mg/ml of the internal standard (L-2-chlorophenylalanine). The LC–MS analysis was performed on a Thermo UHPLC-Q Exactive HF-X system equipped with an ACQUITY HSS T3 column (100 mm × 2.1 mm i.d., 1.8 μm; Waters, USA). The chromatographic conditions were as follows: the mobile phase consisted of 0.1% formic acid in water:acetonitrile (95%:5%) (solvent A) and 0.1% formic acid in acetonitrile:isopropanol:water (47.5%:47.5%:5%) (solvent B). The flow rate was 0.40 mL/min, and the column temperature was 40℃. The injection volume was 3 μl. The MS conditions were as follows: The mass spectrometric data were collected using a Thermo UHPLC-Q Exactive HF-X Mass Spectrometer equipped with an electrospray ionization source operating in positive and negative modes and under the optimal conditions [source temperature, 425 ℃; sheath gas flow rate, 50 arb; aux gas flow rate, 13 arb; ion-spray voltage floating, − 3500 V in negative mode and 3500 V in positive mode; and normalized collision energy, 20–40–60 V rolling for MS/MS]. The full MS resolution was 60,000, and the resolution of MS^2 was 7500. Data were acquired using the data-dependent acquisition mode. Detection was performed over a mass range of 70–1050 m/z. Raw LC–MS data were pretreated using Progenesis QI (Waters Corporation, Milford, USA) to produce a three-dimensional data matrix for filtering the internal standard peaks and other known false-positive peaks (noise, column bleed, and derivatized reagent peaks). Metabolite identification was performed using the HMDB database (http://www.hmdb.ca/). Subsequently, the data matrix was processed as follows: (i) at least 80% of the metabolic features detected in any set of samples were retained. After filtering, the minimum metabolite value was estimated for specific samples with metabolite levels below the lower limit of quantification, and each metabolic signature was normalized to the sum, (ii) the response intensities of the sample mass spectrometry peaks were normalized using the sum normalization method, and (iii) the variables of QC samples with a relative standard deviation > 30% were excluded and log10-logarithmized to obtain the final data matrix for subsequent analysis.

Transcriptomic analysis of small and large intestine contents via Illumina sequencing

Total RNA was extracted from the small and large intestinal tissues using RNeasy Universal Kits (QIAGEN, Catalog no. 73404) according to the manufacturer's instructions. RNA quality was determined using 5300 Bioanalyser (Agilent) and ND2000 (NanoDrop Technologies). High-quality RNA samples (OD260/280 = 1.8–2.2, OD260/230 ≥ 2.0, RIN ≥ 6.5, 28S:18S ≥ 1.0, > 1 μg) were used to construct the sequencing library using Illumina NovaSeq Reagent Kit according to Illumina's library construction protocol. cDNA fragments of 300 bp were size-selected on 2% Low-Range Ultra Agarose and amplified by PCR using Phusion DNA polymerase (NEB) for 15 cycles. The RNA-seq library was sequenced using the NovaSeq 6000 system with assistance from Majorbio Bio-Pharm Technology Co., Ltd. (Shanghai, China). The initial processing of raw data was performed using FASTQ under default parameters. Subsequently, clean reads were assembled and mapped with the reference genome (Macaca mulatta Mmul_10) using StringTie (version 2.2.0) HISAT3-N. The expression level of each transcript was calculated according to the transcripts per million reads method using RSEM (version 1.3.3) to normalize and quantify gene abundance. Differentially expressed genes (DEGs; $|\log_2^{FC}| \geq 2$ and FDR ≤ 0.05) were identified using the R statistical package software EdgeR (Empirical Analysis of Digital Gene Expression in R). Functional enrichment analysis, including GO and KEGG, was performed to determine gene function (GO) and involved pathways (KEGG) using GOATOOLS and KOBAS, respectively.

Results

Variations in histopathologic changes in gastrointestinal tissues caused by CHIKV infection

To confirm the successful construction of the NHP model of CHIKV infection, whole blood was sequentially collected for 7 days for viremia testing. The results showed that the peaks of viremia reached the first 1–2 days post-infection of rhesus macaques and resolved within 4 days (Fig. 1B), consistent with previous trends in the rhesus macaque model of CHIKV infection [23]. To further understand the effects of CHIKV infection on the digestive system, tissues from nine fragments of the GI tract were harvested for further analysis to evaluate histopathological damage (Supplemental Figure S1A). The results showed that in the GI system, CHIKV infection may have the potential to damage the stomach, Peyer's patch, and part of the large intestine (descending colon and rectum), mainly including the infiltration of inflammatory cells and necrolysis of the mucosal epithelium. However, this was not significant (Fig. 1C and Supplemental Figure S1A). GI tract function was evaluated using AB-PAS staining for mucin (goblet cells) (Fig. 1D). Except in the duodenum, mucin levels increased in both the small and large intestines, especially in the cecum (significantly higher), after CHIKV infection. These results revealed that although arboviruses, such as CHIKV, cause muscle infections, they also cause mild variations in the histopathological changes in the GI system. However, more animal numbers are needed for validation.

CHIKV infection shows the potential to affect fecal microbiota

We hypothesized that GI damage caused by CHIKV infection may affect the gut microbiota. To test this hypothesis, we first characterized fecal microbial dynamics before and after CHIKV infection for 7 days through high-throughput sequencing of the fecal microbial 16S ribosomal RNA gene (V4–V5) to explore trends in fecal microbial changes. The results showed that CHIKV infection did not cause significant differences in alpha diversity, including community richness (Sobs index) and diversity (Shannon index). However, the community richness of fecal microorganisms tended to continuously decrease after infection. Correlation analysis further validated the negative correlation between viremia (viral load) and Sobs index (Fig. 2A). Furthermore, partial least squares discriminant analysis (PLS-DA) showed that after infection, fecal microorganisms had a tendency to form a cluster that was (non-significantly) distinct from days 0, especially on days 1–3 (Fig. 2B). This may indicate that CHIKV infection slightly altered the microbial community structure in rhesus monkey feces. At the genus level, *Prevotella* and *Christensenellaceae_R-7_group* had the highest abundance in feces. Notably, after infection, among the top 35 genera, the abundance of *Prevotella*, *Sarcina*, *Parabacteroides*, and *f_Muribaculaceae* gradually increased throughout infection and showed a positive correlation with viremia (high viral load). The opposite trend was observed for *Anaerostipes* and *Lactobacillus*. Furthermore, *Akkermansia* showed a high increase in abundance during days 1 to 3 and declined during days 4 to 7 post-infection (Fig. 2C). These results indicated that fecal microbiota (composition and structure) may be affected by CHIKV infection, particularly during the peak phase of viremia. However, these data are only representative of the terminal end of the intestine.

Altered composition and function of GI microbiota in rhesus monkeys infected with CHIKV

To compensate for the underrepresentation of the fecal microbiome, metagenomics analysis of the microbiome in the small intestine (duodenum, jejunum, and ileum) and large intestine (cecum, ascending colon, transverse colon, descending colon, and rectum) contents was conducted to further characterize the overall microbial landscape of the GI tract after CHIKV infection.

PCoA showed infection-induced alterations in the microbiota of the small and large intestinal segments (PERMANOVA, $P < 0.05$, $R^2 > 0.5$) (Fig. 3A). The composition analysis of microbes at the species level showed that after CHIKV infection, among the high-abundance species (top 30), *Butyricicoccus intestinisimiae*, *Streptococcus lutetiensis*, *Bacilli bacterium*, *Gemmiger formicilis*, and *Oscillospiraceae bacterium* showed significant decreases in abundance. *Prevotella copri* and *Bacteroides fragilis* significantly increased in abundance, particularly in the small intestine (Fig. 3B). Moreover, the abundance of many probiotic organisms, such as *Lactobacillus animalis*, *Lactobacillus salivarius*, and *Lactobacillus fermentum*, decreased post-infection (Supplemental Figure S2A). Furthermore, the occurrence of GI, endocrine, nutritional, and metabolic diseases was elevated in the large intestines of the infected monkeys. However, animal food digestion declined significantly in both the small and large intestines post-infection (Supplemental Figure S2B). Annotation from the virulence factors of the pathogenic bacteria database showed that a large number of virulence factors were up-regulated after infection, especially in the small intestine (Supplemental Figure S2C). Analysis of the contribution of virulence factors (top 5 in abundance) with significantly different (top 10) microbial species indicated that *Prevotella*, *Bacteroides fragilis* (small intestine), and *Clostridium_sp.* (large intestine) had the highest contribution to these virulence factors related to inflammatory signals, inflammatory responses, and pro-inflammatory responses (Supplemental Figure S2D). Moreover, several enzyme functions,

(See figure on next page.)

Fig. 2 Characteristics of the alterations in fecal microbiome in CHIKV-infected monkeys within 7 days. **A** Left, comparison of the Shannon index of fecal microbes at 0 dpi, 1–3 dpi, and 4–7 dpi after infection; middle, comparison of the Sobs index of fecal microbes at 0 dpi, 1–3 dpi, and 4–7 dpi after infection. Right, correlation between viral loads (three time periods) and alpha diversity. Levels of correlation were expressed by color density in the scale bar above. Correlations were evaluated using the Spearman correlation coefficient. values of the correlation coefficient are shown in the box. **B** Above, partial least squares discriminant analysis (PLS-DA) of fecal microbiota at 0 dpi and 1–3 dpi. Below is the PLS-DA of fecal microbiota at 1–3 dpi and 4–7 dpi. Significant differences among clusters were analyzed using PERMANOVA (permutational analysis of variance). R^2 was used to interpret the degree of difference among the groups. Statistical significance was set at $P < 0.05$. **C** Left, heatmap of composition and structure of fecal microbes at 0 dpi, 1–3 dpi, and 4–7 dpi at the genus level (top 35). Red genus, increase in relative abundance compared to 0 dpi; Green genus, decrease in relative abundance compared to 0 dpi. Right, heatmap of correlations between viral loads (three time periods) and the abundance of specific microbiomes (top 35). Levels of correlation were expressed by color density in the scale bar above. Correlations were evaluated using the Spearman correlation coefficient. Taxon of fecal microbiota as follow: o__: Order; f__: family

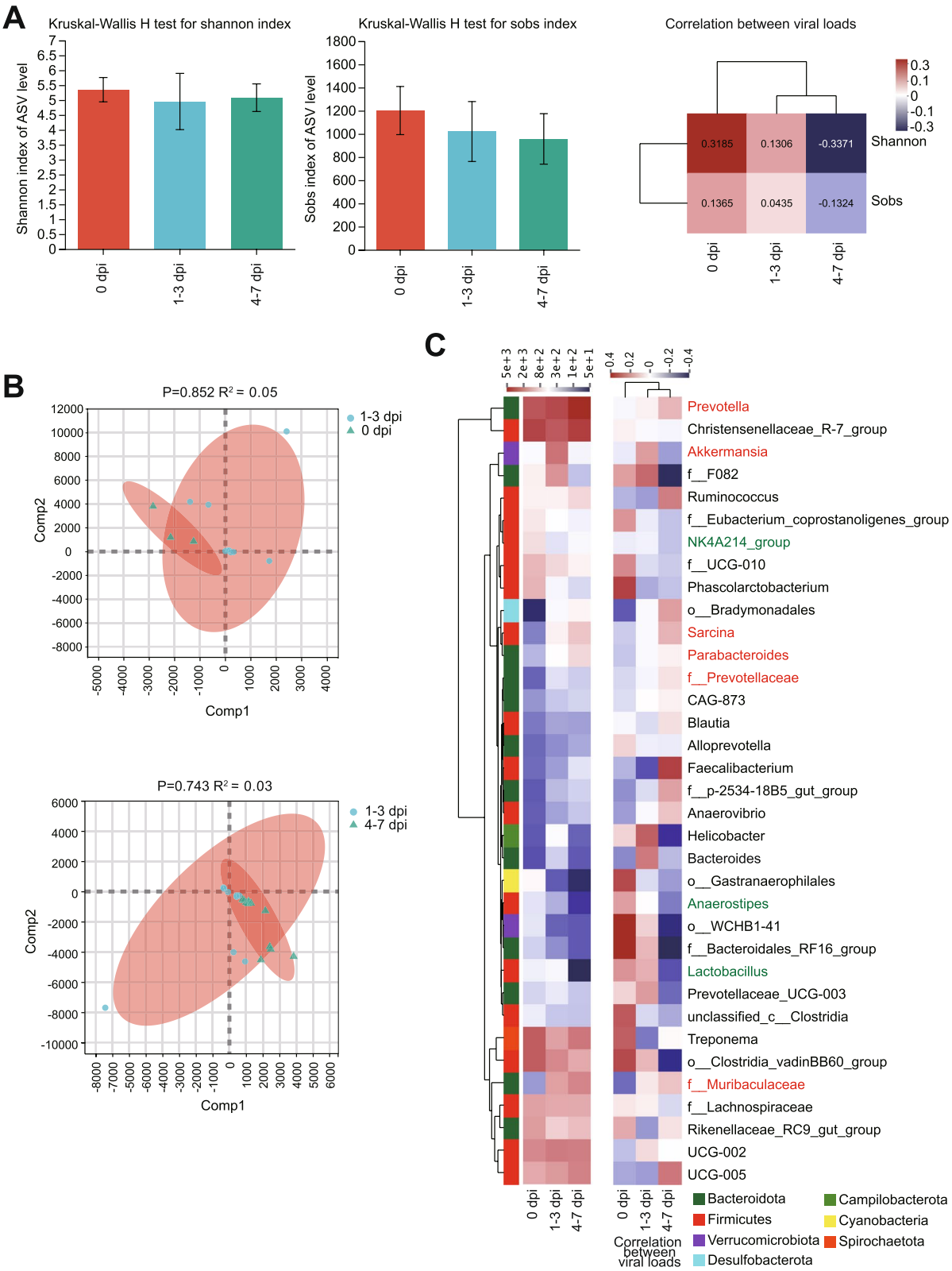

Fig. 2 (See legend on previous page.)

including those of GT2, GH2, GT41, and EC1 (top 5 in abundance), were up-regulated in the small intestine after infection. *Bacteroides fragilis* had the most contribution to GT2 (β-1,3 galactosyltransferase) and GT41 (UDP-GlcNAc) (Supplemental Figure S2D).

Furthermore, we evaluated whether the CHIKV infection caused mechanical damage and stimulated intestinal epithelial repair. Immunofluorescence staining for zonula occludens protein 1 (ZO-1) and epithelial cell adhesion molecule (EpCAM) was conducted in each GI segment (Fig. 3C and Supplemental Figure S1C). We observed that the expression of ZO-1 (except in the rectum and Peyer's patch) and EpCAM (except in the ileum, rectum, and Peyer's patch) increased in most of the GI segments after CHIKV infection at 7 dpi. Collectively, these results demonstrated that CHIKV infection results in an altered structure and composition of the GI microbiota, especially with the high abundance of *Prevotella*, a decrease in probiotics, and an increase in virulence factors. CHIKV infection may stimulate intestinal epithelial repair but does not cause substantial mechanical damage. We hypothesize that this may be related to the sampling period (7 dpi) after infection.

Distinct profiles of GI metabolites in rhesus monkeys post-CHIKV infection

We hypothesized that alterations in the GI microbiota may lead to changes in metabolic products, followed by indirect effects on the host immune system. Therefore, non-targeted metabolomics of the intestinal contents via LC–MS and a combined analysis of metagenomics and metabolomics were conducted to investigate the possible relationship between metabolites and microbes. First, PLS-DA clustering confirmed the changes in metabolites after CHIKV infection. Although the clusters were not clearly separated, metabolites in the small and large intestines formed distinct clusters after infection (Supplemental Figure S3A). Differential metabolite screening via the analysis of variables important in projection (VIPs) identified tyrphostin 47 and nigakinone in both the small and large intestines, the relative abundance of which was significantly increased in the GI tract of infected monkeys. However, bargustanine and lithocholic acid glucuronide levels were significantly decreased in the large and small intestines, respectively. Moreover, gamma-glutamylcysteine levels significantly increased in the small intestine (VIP > 4) (Fig. 4A, B). The functions of these differential metabolites were significantly enriched ($P < 0.05$) in autophagy, infection, and glycosylphosphatidylinositol biosynthesis in the large intestine and ferroptosis, secondary bile acid biosynthesis, and glutathione metabolism in the small intestine (Supplemental Figure S3B).

Further, we conducted a weighted gene co-expression network analysis (WGCNA) of metabolites in each intestinal segment and screened for the top 20 hub metabolites for VIP clustering in the green and turquoise (large intestine) and brown and grey (small intestine) modules. We identified lithocholic acid glucuronide and gamma-glutamylcysteine in the small intestine (Fig. 4C and Supplemental Figure S3C). Consistently, these hub metabolites were mainly enriched in the digestive system (bile secretion, protein digestion, and absorption); amino acid metabolism (tryptophan metabolism and lysine degradation) was enriched in the small intestine, and cancer: overview (choline metabolism) and lipid metabolism (glycerophospholipid metabolism, biosynthesis of unsaturated fatty acids) were enriched in the large intestine (Supplemental Figure S3D). Subsequently, we analyzed the variations in SCFAs, tryptophan, and bile acids. The results showed that after infection, valeric acid levels were significantly increased in the small and large intestines, and L-tryptophan, tryptophol, and tryptophan-tyrosine levels were significantly up-regulated in the large intestine. Importantly, consistent with our results of functional annotation enrichment, the abundance of multiple bile acid metabolites, such as cholic acid, deoxycholic acid, taurochenodeoxycholic acid, and lithocholic acid glycine conjugate (in the small intestine) and 7a-Hydroxy-cholestene-3-one and lithocholic acid 3-O-glucuronide (in the large intestine), were significantly increased ($P < 0.05$) in the GI system after infection (Fig. 4D).

(See figure on next page.)

Fig. 3 Microbial beta-diversity, composition, and dominant microorganisms in the GI contents of CHIKV-infected animals. **A** Principal coordinate analysis (PCoA) of the microorganisms in the GI contents. Significant differences among clusters were analyzed using PERMANOVA (Permutational analysis of variance). R^2 was used to interpret the degree of difference among the groups. Statistical significance was set at $P < 0.05$. **B** Composition and structure of microbes in the GI content at the species level. The outside left ribbons indicate the level of the genus belonging to this species. Red species, increase in relative abundance of microbes in the large or small intestine compared to the negative control (NC) group. Green genus, decrease in the relative abundance of microbes in the large or small intestine compared to the NC group (Kruskal–Wallis *H* test; $^*P < 0.05$). Taxon of fecal microbiota as follows: o__: Order; g__: genus. **C** Above, the epithelial integrity of the GI tract was determined via immunofluorescence staining of the zonula occludens (ZO-1) protein and epithelial cell adhesion molecule (EpCAM) as described in the Materials and Methods section, *(Welch's *t*-test; $^*P < 0.05$, $^{**}P < 0.01$, $^{***}P < 0.005$, $^{****}P < 0.001$). Below are representative images (Supplemental Figure S1C)

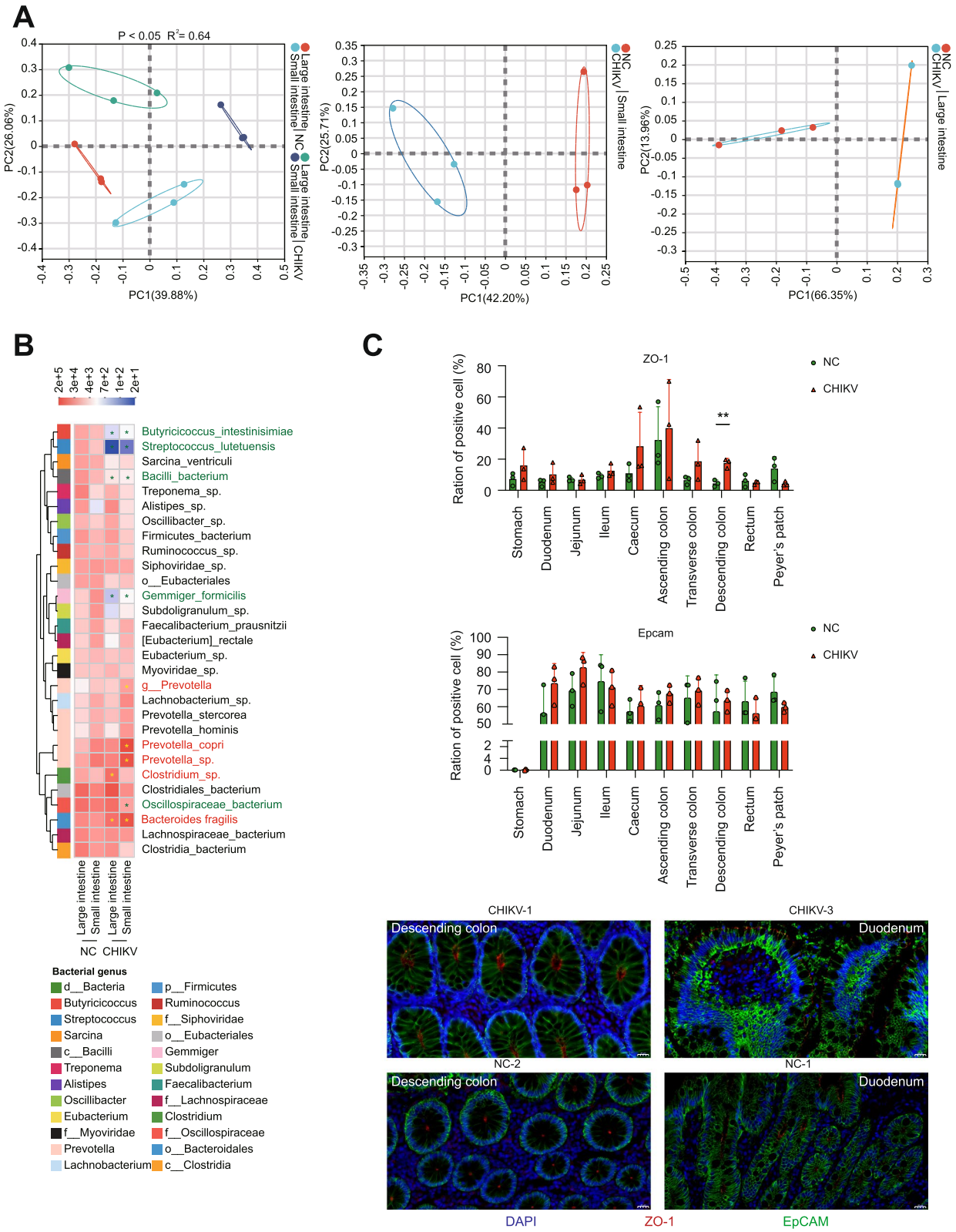

Fig. 3 (See legend on previous page.)

Redundancy and matrix correlation analyses were performed to further explore the correlations between the GI microbiota, especially microbial species with significant differences, and metabolite changes. The results of the correlation analysis showed that, in the small and large intestines, metabolites with the top five VIP values had a higher correlation with microbial species (significantly different), except for bargustanine. Among the species that significantly increased in abundance, *Prevotella sp.* showed a positive correlation with 3a,6b,7b-trihydroxy-5b-cholanoic acid ($P < 0.05$), glabric acid, 7,8-dihydropteroic acid, and tryphostin 47 but showed a negative correlation with gamma-glutamylcysteine. After CHIKV infection, most of the metabolites (except for 3a,6b,7b-trihydroxy-5b-cholanoic acid) were positively correlated with the up-regulated microbial species, such as *Bacteroides fragilis* and *Clostridium sp.* and vice versa (Supplemental Figure S4A).

Furthermore, among the SCFAs and tryptophan metabolites, *Prevotella sp.* showed a significant positive correlation with up-regulated indoleacrylic acid and L-tryptophan levels. However, *Oscillospiraceae bacterium, Bacilli bacterium*, *Gemmiger formicilis*, *Butyricicoccus intestinisimlas*, and *Streptococcus lutetiensis* showed significant positive correlations with SCFAs and breakdown products such as valeric acid, 2-(20-hydroxyicosa-5,14-dienoylamino)acetic acid, and {4-[4-(6-carbamoyl-3,5-dimethylpyrazin-2-yl)phenyl] cyclohexyl}acetic acid. Moreover, *Oscillospiraceae bacterium* and *Bacilli bacterium* showed positive correlations with several increased tryptophan metabolites, such as tryptophol, 3-hydroxykynurenamine, and tryptophan-tyrosine (Supplemental Figure S4B–D). These results suggest that the alteration of the GI microbiota by CHIKV infection also induces changes in metabolites that are involved in the regulation of host metabolism and immune responses.

Immune-related genes differentially activated in GI tissues post-CHIKV infection

To further understand the GI response to CHIKV infection, we performed a transcriptomic analysis of each GI fragment and whole blood from monkeys. Exactly 3,157,165,438 clean reads, covering 469,186,616,860 bases, were produced from 66 specimens of each GI tissue and blood sample from NC and CHIKV-infected rhesus monkeys. The Q30 values of all the samples were above 90% (minimum, 93.5%), and the ratios of clean reads mapped to the reference genomes were over 80%. Exactly 1770 DEGs were identified ($P < 0.05$; FC ≥ 2), of which 945 and 816 were up- and downregulated, respectively, in CHIKV-infected monkeys. All DEGs were significantly enriched in allograft rejection, autoimmune thyroid disease, RA, and cytokine-cytokine receptor interactions. Moreover, some DEGs were enriched in the NF-kappa B signaling pathway and inflammatory bowel disease (IBD) (Supplemental Figure S5A). Notably, DEGs in the GI tract were significantly up-regulated for multiple chemokine (*CCL3*, *CCL20*, *CXCL1*, and *CXCL5*) and interleukin (*IL-1*, *I L-6*, *IL-11*, and *IL-1β*) genes but were significantly down-regulated for *IFN-γ* in the RA pathway after CHIKV infection. Cluster genes in the Th17-activated osteoclast pathway, such as *IL-6*, *IL-17A*, and *ATP6V0C*, were significantly up-regulated; however, no differential expression of *RANK* or *RANKL* was observed in the GI tract (Fig. 5A).

Furthermore, analysis of the gene set clustered all DEGs into 10 subclusters according to the expression trends. Among the subclusters, DEGs in subclusters 1, 3, and 6 and subclusters 2 and 4 were upregulated and downregulated, respectively (Supplemental Figure S5B). After infection, the primary functions of the up-regulated subclusters were shigellosis (subcluster 1); IL-17 signaling pathway, TNF signaling pathway and rheumatoid arthritis (subcluster 3); and glutathione metabolism (subcluster 6) (Supplemental Figure S5C). Therefore, we further analyzed gene expression in the protective immunity

(See figure on next page.)

Fig. 4 Distinct profiles of GI metabolites in rhesus monkeys post-CHIKV infection. **A** Left, volcano plot of differential metabolites in the large intestine. Right, volcano plot of differential metabolites in the small intestine. **B** Left, heatmap of the abundance of metabolites (top 10 VIP values) in the large intestine. Right, heatmap of the abundance of metabolites (top 10 VIP values) in the small intestine. Expression levels are indicated by the color density of the scale bar. **C** Weighted gene co-expression network analysis (WGCNA) was performed to identify the metabolites and their correlations with fragments of the GI tract to identify hub metabolites. In the top panel, metabolites that were correlated with fragments of the GI tract were clustered to form several modules, as indicated (minModuleSize:30; minKEMtoStay:0.3; mergeCutHeight:0.25; soft power:8). Correlation of the modules with specific phenotypes (metabolites in each GI segment of the infected and negative control (NC) monkeys) are presented. The numbers in the left column (modules) indicate the number of metabolites in the module. The numbers in the middle box indicate the correlation coefficients and *p*-values (in parentheses) between the modules and phenotypes. Correlation levels were differentiated by the color of the scale bar above (red for positive correlation and green for negative correlation) (Supplemental Figure S3C). **D** Heatmap of the metabolite expression of representative SCFAs, tryptophan, and bile acids (red, increased relative abundance compared to the NC group; green, decreased relative abundance compared to the NC group; Kruskal–Wallis *H* test; $^*P < 0.05$)

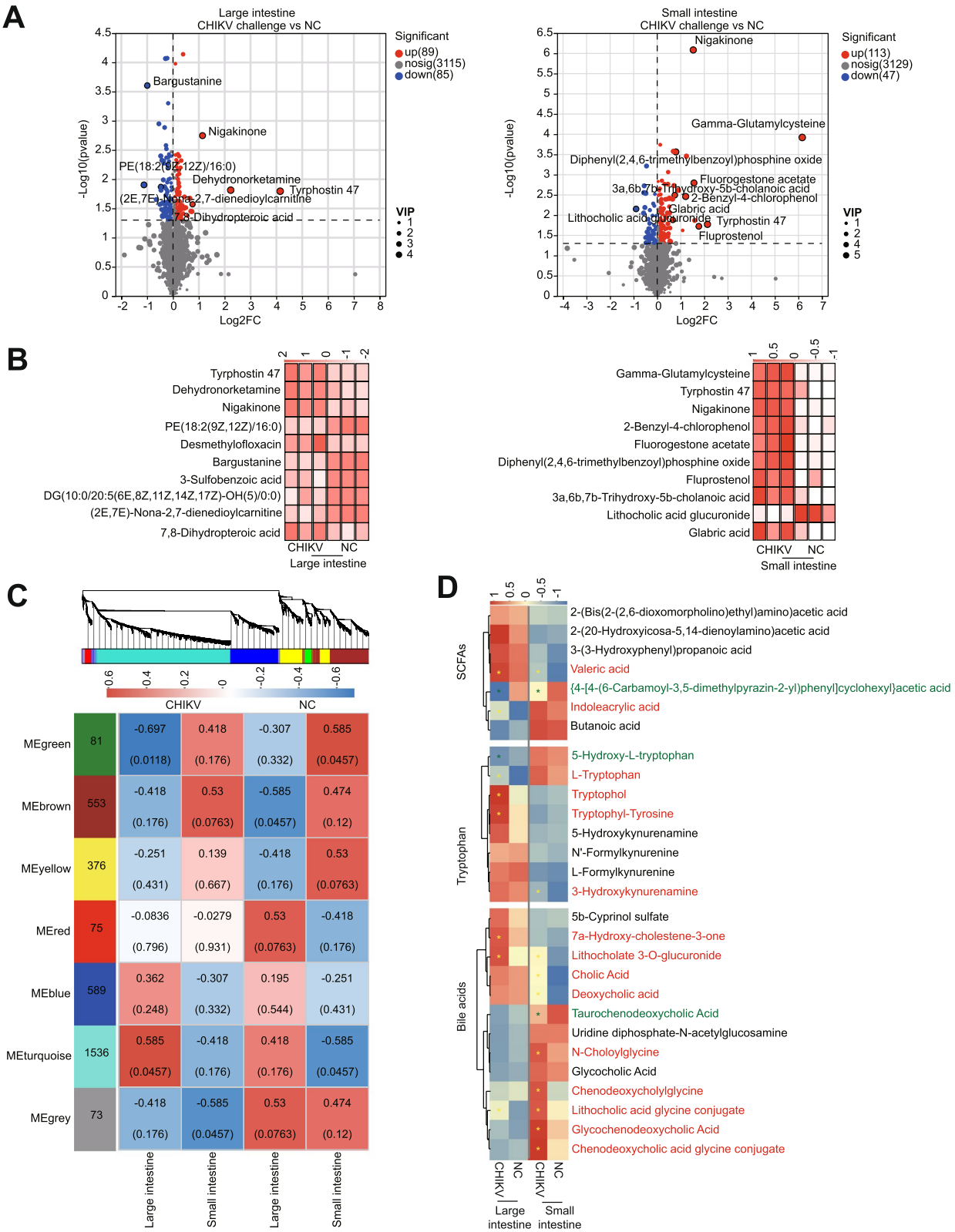

Fig. 4 (See legend on previous page.)

of the IL-17 pathway. *IL17A* (stomach and small and large intestine), *IL17B* (stomach and large intestine), *IL17C* (stomach and large intestine), *IL1β* (stomach and large intestine), *IL6* (small and large intestine), *CXCL1* (stomach and large intestine) and *CXCL8* (stomach and large intestine) were up-regulated in the GI tract of infected monkeys, especially in the segment (stomach and large intestine) with the most severe pathology (Fig. 5B). Subsequently, to fully understand the inflammatory response of the GI tract after CHIKV infection, transcriptomic analysis of all interleukin and inflammasome genes in blood and GI fragments from monkeys was performed. The result showed that interleukin genes were up-regulated primarily in the stomach (*IL-1α*, *IL-1β*, *IL-10*, *IL-17A*, *IL-19*, *IL-20*, *IL-22*) and small intestine (*IL-21*, *IL-22*, *IL6*, *IL10*, *IL-17A*) after CHIKV infection. However, most immunoregulatory cytokines were down-regulated in Peyer's patches. The expression of inflammatory cytokines *IL-17A* and *IL-2* was up-regulated in the stomach and small and large intestines of infected monkeys. Meanwhile, *IL-1α*, *IL-1β*, and *IL-6* expression were up-regulated in the blood, stomach, and large intestine of infected monkeys (Fig. 5C). Furthermore, CHIKV infection resulted in the down-regulation of *NLRP1*, *NLRP2*, and *NLRP3* expression in both the blood and GI tract, whereas *NLRP10*, *NLRP11*, *NLRP8*, *NLRP5*, and *NLRP14* expression was up-regulated in the stomach, large intestine, and Peyer's patches.

To further illustrate immune cell infiltration to provide more granularity regarding viral infection, host immunity, and cytokine milieu after CHIKV infection in the GI tract, CD68 + and CD4 + signatures were used to detect macrophages and T lymphocytes, respectively (Supplemental Figure S6B). We found that CHIKV-infected monkeys showed an increased number of CD4 + cells in the stomach (significant), jejunum, cecum, transverse colon ($P < 0.05$), rectum, and Peyer's patches. Furthermore, the infected rhesus monkeys exhibited an increase in CD68 expression in the stomach ($P < 0.05$), cecum, descending colon ($P < 0.05$), rectum ($P < 0.05$), and Peyer's patches.

Considering the potential role of double-stranded RNA viruses, especially CHIKV, and bacterial lipopolysaccharides in the host in interferon modulation, we comprehensively analyzed all IFN genes and genes in the MYD88 IFN pathway in the GI tract after infection. The results showed that toll-like receptor (TLR) genes were only up-regulated in the stomach (*TLR3*, *TLR4*, and *TLR7*) and small intestine (*TLR3*) of the infected monkeys. However, all were down-regulated in the large intestine and Peyer's patches. Correspondingly, *TRAM1*, *TRAM2*, and *TRAF3* and *IFN-γ*, *IFNG1*, *IFNG2*, *IFGNR1*, and *IFGNR2* were up-regulated in the stomach and small intestine, respectively (Fig. 5D, E).

Finally, the gene expressions of *G3BPs* (Ras GTPase-activating protein-binding protein 2) and *MXRA8* (Matrix remodeling-associated protein 8), which are important for CHIKV infection, and *FHL1* (four-and-a-half LIM domain protein 1) and *MSR1* (Macrophage scavenger receptor 1), which are important for CHIKV inhibition, were analyzed in fragments of the GI tract after CHIKV infection. We demonstrated that all host factors were expressed in the GI tract. The major receptor *MXRA8* was primarily and abundantly expressed in fragments of the stomach and large intestine (upregulated after infection). However, *MXRA8* mRNA was also found in other fragments of the GI tract. Furthermore, the expression of *G3BP2* (except in the duodenum and ileum) and *FHL1* was down-regulated in the GI tract. Although *MSR1* expression was up-regulated in the colon and ileum, it showed lower expression in the GI tract (Supplemental Figure S6A).

Therefore, CHIKV infections may have altered the expression levels of major viral receptors in the GI tract. Still, multiple chemokine and interleukin genes in the Th17 RA pathway were transcriptionally activated. Particularly, the stomach, cecum, colon, rectum, and Peyer's patch, which are more damaged after infection, exhibited high inflammation, which may contribute to controlling viral infections or regulating systemic inflammation by the "gut-joint axis."

(See figure on next page.)

Fig. 5 Transcriptomic profile of the fragments in the GI tract post-CHIKV infection. **A** Enrichment map of the differentially expressed genes (DEGs) in the rheumatoid arthritis (RA) pathway. Genes in the red box represent the DEGs enriched in this study. The green arrows indicate genes with decreased expression (mean) compared to the negative control (NC) group; the red arrows indicate genes with increased expression (mean) compared to the NC group. (*$P < 0.05$; $Log_2^{FC} > 2$). At 7 dpi, the animals were euthanized and dissected. Blood and tissue samples from the GI tract were collected for RNA sequencing and transcriptomic analysis, followed by further analysis of genes related to the function of **B** protective immunity of the IL-17 pathway; **C** interleukins; **D** interferons (IFNs); and **E** IFN genes of the MYD88 pathway. Each panel (**B**, **C**, **D**, and **E)** comprises two parts. The heatmap (red-blue) on the left of each panel shows the relative expression of genes (RPKM), and the expression levels are indicated by the color scale bar above. The heatmap (red-green) on the right shows the log_2 fold change (infected monkeys vs. NC) of the values of differentially expressed levels (mean), and the expression levels are indicated by the color scale bar above

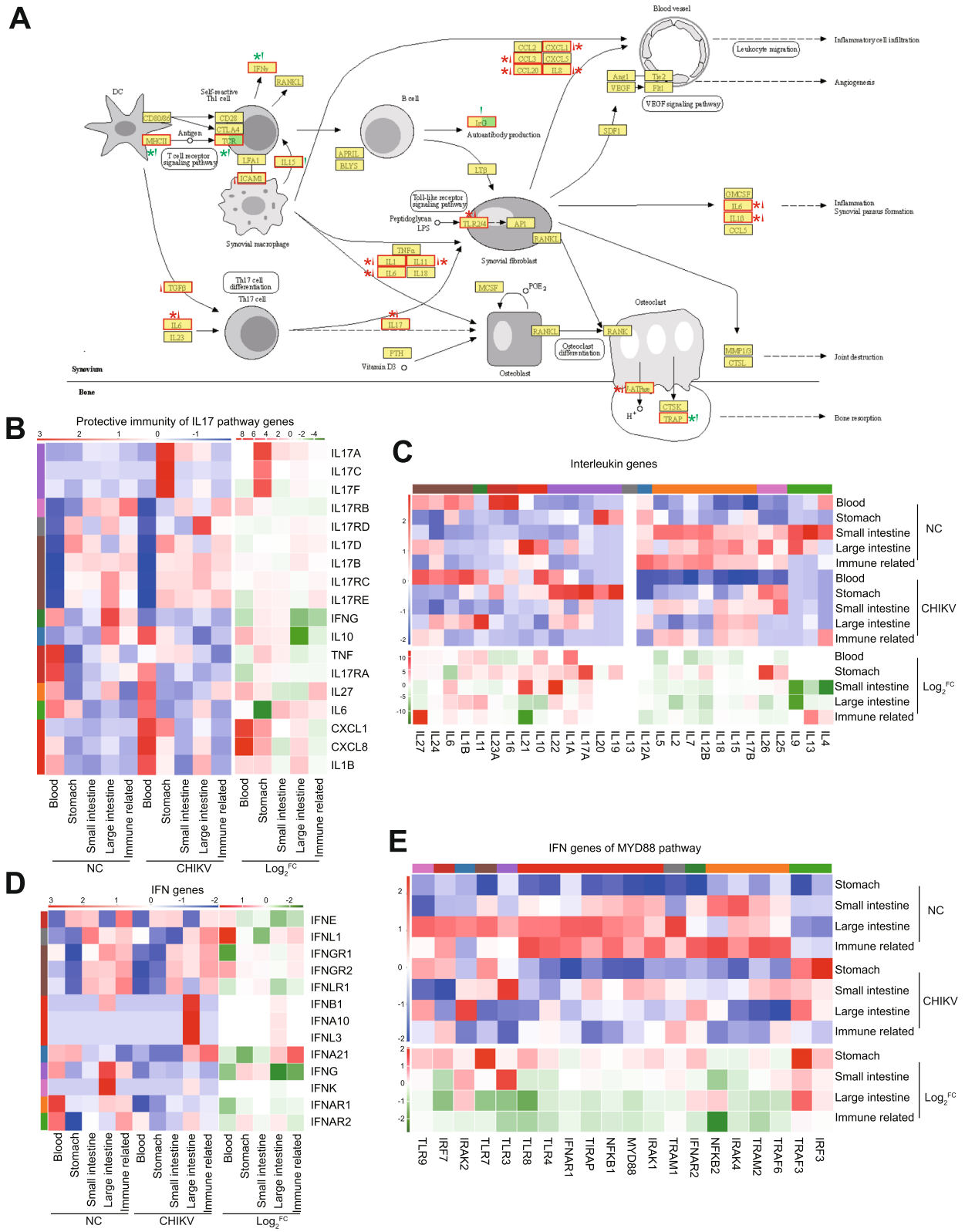

Fig. 5 (See legend on previous page.)

Discussion

CHIKV has been globally transmitted to more than 100 countries and regions, causing millions of infection cases and a significant economic burden in affected areas [24]. However, no drugs and only one vaccine (IXCHIQ) have been officially approved for the prevention and treatment of CHIKV infection [10]. Therefore, a comprehensive analysis of the immunological and virological mechanisms is an active research area. CHIKV infection leads to crippling musculoskeletal inflammatory diseases (persistent arthralgia and arthritis) similar to RA [10]. This suggests that the development and progression of CHIKV infection may be linked to gut immunity and microbiome. In this study, we performed an integrated analysis of fecal and GI microbiota, microbial metabolism, and host immune responses in the GI tract after CHIKV infection based on an established NHP model. We observed that CHIKV infection, although causing only minor damage to the digestive system, resulted in alterations in microorganisms and metabolites in the GI tract. Our comprehensive analysis revealed that the GI tract and microbiota may be involved in immunomodulation after CHIKV infection (influencing the immune response).

Previous studies have shown that the primary target organs of CHIKV infection in rhesus monkeys are the liver, spleen, joints, and muscles [25]. In this study, we showed that in the GI tract, the major receptors (host factors), *MXRA8*, *FHL1*, and *NAP1L1*, were highly expressed (especially in the stomach and colon segments). MXRA8 (up-regulated after infection) is the major CHIKV receptor (directly interacting with the CHIKV envelope) that interacts with the E1-E2 trimerization protein and facilitates CHIKV invasion of host cells [26]. Furthermore, FHL1 (down-regulated after infection) interacts with the hypervariable domain in CHKnsp3 to inhibit viral replication [27]. The stomach, descending colon, and rectum of CHIKV-infected monkeys in this study showed greater pathological damage and increased ZO-1 expression, which may reflect the potential of CHIKV to infect GI tissues, especially the stomach and large intestine, and stimulate the repair of GI tissues following injury. However, the viral loads were not detected in GI tissues and feces, and EpCAM expression was increased. The peak time of viremia (viral accumulation was measured) in the NHP infection model in this study (1–3 dpi) aligned with that of the study by Messaoudi et al. that detected gradual recovery at 3 dpi after infection. Therefore, we speculate that this may be related to the non-acute phase of CHIKV infection [23].

In this study, fecal microbiota did not significantly change post-CHIKV infection, and only trends could be observed. The fact that fecal microbiota was underrepresented might have been the main cause of this result [28]. In the feces, after CHIKV infection, the abundance of *Akkermansia* increased (positively correlated with high viral loads) at 1–3 dpi and then decreased. *Prevotella* and *Muribaculacea* abundance consistently increased (positively correlated with high viral loads), and that of microorganisms associated with SCFA metabolism, such as *NK4A214_group* and *Anaerostipes*, also decreased (negatively correlated with high viral loads) [29]. A high abundance of *Prevotella* has been shown to decrease SFCA levels and is related to Th17-mediated mucosal inflammation [30, 31]. *Muribaculaceae* contributes to the inhibition of intestinal barrier dysfunction, IBD, and lipid metabolism disorder [32]. *Akkermansia* is an intestinal probiotic that decreases in abundance with enteritis progression. Bae et al. found that a decrease in *Akkermansia* abundance leads to thinning of the intestinal mucosal layer and compromises the barrier function [33]. Furthermore, most GI tract fragments at 7 dpi showed an increase in the number of mucin-secreting goblet cells compared to those in the NC group. This may reflect a synergistic host defense against viral infections by microbes [34]. The abundance of microorganisms in the GI tract further compensates for the underrepresentation of fecal microorganisms [28]. Consistent with the fecal microbiota results, the abundance of multiple species of *Prevotella*, especially *Prevotella copri*, increased in both the small ($P < 0.05$) and large intestines after CHIKV infection. The positive relevance of highly abundant *P. copri* to RA and ankylosing spondylitis has been demonstrated repeatedly because of the sequence homology between RA-specific autoantigens (N-acetylglucosamine-6-sulfatase and filamin A) and epitopes (sulfatase proteins) of *P. copri* proteins [35]. The epitopes are also regarded as potential biomarkers for RA and SA [36, 37].

Moreover, *Prevotella* is known to activate various immune cells/factors such as mucosal T cells, Th17, and IFN-γ [38]. IL-17 is mainly secreted by Th17, and IL-17A induces epithelial cells to secrete pro-inflammatory cytokines and chemokines to maintain inflammation and promote the formation of fibroblast-like synoviocytes and osteoclasts, which trigger osteoarticular inflammation and bone damage [39, 40]. The contribution of IL-17 to persistent joint inflammation after CHIKV infection has been reported [41–43]. In this study, after CHIKV infection, IL-17A and IL-17B expression were up-regulated in the GI tract. Moreover, 10 DEGs were enriched in the RA pathway of Th17. The number of CD4 + T cells (important effectors of joint inflammation) also increased, consistent with the findings of Liu et al. [42].

Additionally, the key feature of the dominance of *P. copri* in the GI tract was the transfer of *Bacteroides* [38]. In this study, we found a significant increase in the

abundance of *Bacteroides fragilis* in the large intestine after infection. On the one hand, *Bacteroides fragilis* is an important regulatory molecule of Tregs [44]. On the other hand, the function of purine metabolism is significantly reduced in *Prevotella*-dominated microbiomes. A high abundance of *Bacteroides fragilis* can increase dihydrofolate synthesis, which regulates joint inflammation [38]. We hypothesized that the dominant microbial bias caused by CHIKV infection, especially *Prevotella*, may be involved in joint inflammation due to the immune activation of Th17 cells after infection. However, further studies are needed to demonstrate the role of IL-17 in the antiviral response to CHIKV infection, particularly in the gut-joint axis.

Microorganisms associated with the secretion of SCFAs (especially butyric acid) and antimicrobial peptides are down-regulated in the GI tract after infection. These include *Butyricicoccus intestinisimiae* [45], *Oscillospiraceae_bacterium* [46], *Gemmiger formicilis*, and *Strep. lutetiensis* [47, 48]. The abundance of probiotics (*Lactobacillus animalis*, *Lactobacillus salivarius*, *Lactobacillus fermentum*) also reduces. This may partially explain the up-regulation of inflammatory signals, inflammatory responses, and virulence factors following CHIKV infection (Supplemental Figure S2).

Alterations in GI microbes result in metabolic changes that can induce and promote host immune responses [49]. Most of the significantly up-regulated GI metabolites (except gamma-glutamylcysteine) identified in this study were positively correlated with the microbial species that were up-regulated after CHIKV infection. All these metabolites, including tyrphostin 47, nigakinone, and gamma-glutamylcysteine, are involved in dampening inflammation.

The activation of inflammatory signaling and induction of chronic inflammation have been reported to be critically dependent on the activation of MAPK (p38) [50]. Tyrphostin 47 effectively hinders the process of Tyr-phosphorylation within the activation loop of p38 MAPK, thereby mitigating inflammation and upholding homeostasis, and has been demonstrated to hold significant potential for the therapeutic intervention of Shiga toxin-producing bacterial infectious diseases [51]. Nigakinone exerts its anti-inflammatory effects on colonic inflammation by modulating the expression of FXR to regulate the bile acid cycle and inhibit the activation of the NLRP3 inflammatory vesicle complex [52]. Liu et al. demonstrated that nigakinone could alleviate symptoms in rats with colitis induced by dextran sulfate sodium, including an excessive inflammatory response induced by NLRP3 activation and damage to the intestinal mucosal barrier [53]. Consistently, in this study, *NLRP3* was down-regulated throughout the GI tract and blood after infection (Supplemental Figure S5D). Furthermore, the abundance of secondary bile acids and their decomposition products increased significantly. However, the abundance of bile acid 7α-dehydroxylating bacteria *Clostridium sp.* (generation of secondary bile acids) [54] increased significantly in the large intestine after CHIKV infection (Fig. 3B) and showed a positive correlation with nigakinone (Supplemental Figure S4A). Gamma-glutamylcysteine is an intermediate dipeptide in the glutathione synthesis pathway with anti-inflammatory properties. Liu et al. found that, in RA mice, dysbiosis of the intestinal microbiome induced by joint inflammation could up-regulate gamma-glutamylcysteine expression to inhibit cysteinyl asparagine-1 and NLRP3 inflammasome activation and attenuate joint inflammation [55]. This finding strongly aligns with our results.

The impact of virus infection on the host microenvironment has been demonstrated in many studies. Chen et al. found that, respiratory infection with SARS-CoV-2-induced alteration of GI microbiota and metabolites. More importantly, mutant strain with different virulence shows different degrees of disturbance for the host microbiome [56]. Furthermore, Zhang et al. demonstrate that mosquito-transmitted flaviviruses can manipulate host skin microbiota to promote the expansion of acetophenone-producing bacteria in host skin that attracts mosquitoes to enhance the probability of viral dissemination in nature [57]. Taken together, we propose that, although CHIKV is not an enteric virus, CHIKV may increase the systemic burden of inflammation in the GI system of infected animals. Meanwhile, infection-induced alterations in GI microbiota and metabolites may be indirectly involved in gastrointestinal and bone (joint) inflammation modulation after CHIKV infection, such as the modulation of inflammasome and IL-17 inflammatory cytokine levels (Supplemental Figure S6C). However, this study had some limitations. First, antibiotic treatment is essential to clarify the pathogenesis of the GI microbiota in CHIKV infection. Furthermore, the key microbes and metabolites found in this study require further validation. Moreover, osteoarticular inflammation due to CHIKV infection is associated with the duration of infection and patient age [58]. Therefore, additional animals, ideally C57BL/6 mice of different ages, are required to confirm the results of this study.

To the best of our knowledge, this is the first study to systematically explore the GI environment in CHIKV infections using an NHP model. Our results suggest that GI microbiota may provide new insights into the adjuvant treatment of CHIKV infections.

Abbreviations

CHIKV	Chikungunya virus
WA	West African

ECSA	East/Central South African
IOL	The Indian Ocean lineage
Treg	Regulatory T cells
RA	Rheumatoid arthritis
LPS	Lipopolysaccharides
MAMP	Microbe-associated molecules
SCFA	Short-chain fatty acids
PGN	Peptidoglycans
GI	Gastrointestinal
NHP	Non-human primate
ABLS3	Animal biosafety level 3
PBS	Phosphate-buffered saline
PFU	Plaque-forming units
AB-PAS	Alcian blue and Periodic acid-Schiff
OTUs	Operational taxonomic units
H&E	Hematoxylin-eosin staining
ZO-1	Zonula occludes protein 1
EpCAM	Epithelial cell adhesion molecule
PCoA	Principal coordinate analysis
PERMANOVA	Permutational analysis of variance
PLS-DA	Partial least squares discriminant analysis
db-RDA	Distance-based redundancy analysis
PICRUSt2	Phylogenetic Investigation of Communities by Reconstruction of Unobserved States
VIP	Variable important in projection
FDR	False discovery rates
DEGs	Differentially expressed genes
GO	Gene Ontology
KEGG	Kyoto Encyclopedia of Genes and Genomes
WGCNA	Weighted gene co-expression network analysis
IBD	Inflammatory bowel disease
TLR	Toll-like receptors
G3BPs	Ras GTPase-activating protein-binding protein 2
MXRA8	Matrix remodeling-associated protein 8
FHL1	Four-and-a-half LIM domain protein 1
MSR1	Macrophage scavenger receptor 1
MXRA8	Matrix remodeling-associated protein 8
DHF	Dihydrofolate

Supplementary Information

The online version contains supplementary material available at https://doi.org/10.1186/s40168-024-01895-w.

Supplementary Material 1: Supplementary Figure S1. A: Histopathological analysis of pulmonary and GI tissues in rhesus monkeys challenged with CHIKV. At 7 dpi, the animals were euthanized and dissected. The indicated tissues were harvested and processed for H&E staining and histopathological evaluation as described in the Materials and Methods section. The scale bars are 20 μm. Related to Figure 1C. B: At 7 dpi, the animals were euthanized and dissected. Tissues were collected for subsequent analyses. Representative images regarding the IHC analysis of the AB-PAS staining of mucin (goblet cells) are shown here. The scale bars are 20 μm. Related to Figure 1D. C: Representative images for the immunofluorescence staining of zonula occludens protein (ZO-1, red) and epithelial cell adhesion molecule (EpCAM, green) are shown here. The scale bars are 20 μm. Related to Figure 3C. Supplemental Figure S2. A: Heatmap of the relative abundance of intestinal probiotics of microbes in the GI contents of negative control (NC) and CHIKV-infected monkeys. The relative abundance is indicated by the color of scale bar on the left. B: Heatmap showing the functions involved in the disease classes of microbes in the GI contents of NC and CHIKV-infected monkeys. The relative abundance is indicated by the color scale bar on the left. C: Heatmap of the relative abundances of virulence factors and enzyme functions of microbes in the GI contents of NC and CHIKV-infected monkeys. The relative abundance is indicated by the color scale bar on the left. D: Contribution analysis regarding the species and functions (above, virulence factors; below, enzymes) of microbes in the GI contents of NC and CHIKV-infected monkeys. The relative abundance is indicated by the color scale bar in the middle. Supplemental Figure S3. A: Partial least squares discriminant analysis (PLS-DA) of the metabolites in the GI contents. B: Above, KEGG enrichment analysis (level 3) of the metabolites in the contents of the large intestine. Below, KEGG enrichment analysis (level 3) of the metabolites in the contents of the small intestine. * (* $P < 0.05$, ** $P < 0.01$, *** $P < 0.005$). C: Heatmap of the abundance of hub metabolites (the top 10 VIP values) in the large (above) and small (below) intestines, which was obtained via weighted gene co-expression network analysis (WGCNA). Related to Figure 4C. Supplemental Figure S4. A: the metabolites with top 10 VIP values in the large and small intestines. Related to Figure 4B; B: SCFAs; C: tryptophan; D: bile acids). Red species and metabolites: increased after CHIKV infection; Green species and metabolites: decreased after CHIKV infection. Related to Figures 3B & 4B–D. The significance was marked with *(* $P < 0.05$, ** $P < 0.01$, *** $P < 0.005$, **** $P < 0.001$), and the heatmap was plotted using the R pheatmap package. Correlations were evaluated using Spearman's correlation coefficient. Supplemental Figure S5. A: KEGG enrichment analysis of all DEGs at level 3. B: Sub-clustering of the DEGs according to their expression levels. DEGs in subclusters 1, 3, and 6 were up-regulated in infected monkeys compared to negative controls (NCs); DEGs in subclusters 2 and 4 were down-regulated in infected monkeys compared to NCs. C: KEGG enrichment analysis of the DEGs in subclusters 1, 3, and 6. D: Analysis of the genes related to inflammasome function. The heatmap (red-blue) on the left panel shows the relative expression of genes; the expression levels are indicated by the color scale bar above. The heatmap (red-green) on the right shows the $\log_2$ fold change (infected monkeys vs. NCs) of the values of differentially expressed levels (mean); the expression levels are indicated by the color scale bar above. Supplemental Figure S6. A: Heatmap of the gene expression levels of CHIKV host factors and receptors (G3BP2, MXRA8, FHL1, and MSR1). The heatmap (red-blue) on the left panel shows the relative expression of genes; the expression levels are indicated by the color scale bar above. The heatmap (red-green) on the right shows the $\log_2$ fold change (infected monkeys vs. NCs) of the values of the differentially expressed levels (mean); the expression levels are indicated by the color scale bar above. B: CD68+ and CD4+ signatures were used to detect macrophages and T lymphocytes, respectively, using immunofluorescence staining, as described in the Materials and Methods section. Compared with the NC group, a significant difference in cell count in the GI tissues of infected animals was indicated by *Welch's t-test* and plotted using GraphPad Prism 8.0. *(*$P < 0.05$, **$P < 0.01$, ***$P < 0.005$, ****$P < 0.001$). Right: representative images of the immunofluorescence staining of CD4+ (green) and CD68+ (red) cells. C: Summary of the conclusion of this study. This figure was prepared using the online software Figdraw (Copyright No. YUSWT8efe0).

Acknowledgements
We appreciate the services of all the staff at the National Kunming High-level Biosafety Primate Research Center.

Authors' contributions
SL, QS, NZ and YH designed the study. HC, JS, CT and JX wrote the manuscript. HC, CT, JX, BL, JW, YZ, YY, HY, QH, WY, HW, DW and SL performed experiments. HC, JX, CT analyzed data. All authors have read, edited, and approved the final manuscript.

Funding
This study was supported by the CAMS Innovation Fund for Medical Sciences (2021-I2M-1-038, 2022-I2M-CoV19-002, 2021-I2M-1-039), Yunnan Key R&D Project (202103AQ100001), National Key R&D Program of China (2021YFC230170402, 2021YFC0864600, 2020YFA0707602), Project supported by the Foundation for Innovative Research Groups of the National Natural Science Foundation of China (82221004), National Science Foundation of China (32170166), Chinese Central Government for Basic Scientific Research Operations in Commonweal Research Institutes (2021-PT310-007). Technical Innovation Talents of Yunnan Province, Grant/Award Number:202205AD160008. Fundamental Research Funds for the Central Universities (3332022072).

Availability of data and materials
Sequence data that support the findings of this study have been deposited in the NCBI database. Detial is provided within the manuscript.

Declarations

Ethics approval and consent to participate
All animal procedures in this study were approved by the Institutional Animal Care and Use Committee of the Institute of Medical Biology, Chinese Academy of Medical Science (ethics number: DWSP202110006). All experiments involving live CHIKV were conducted at the ABSL-3 laboratory of the National Kunming High-level Biosafety Primate Research Center.

Consent for publication
All authors have consented to publication.

Competing interests
The authors declare no competing interests.

Received: 22 November 2023 Accepted: 30 July 2024
Published online: 30 August 2024

References

1. Schwartz O, Albert ML. Biology and pathogenesis of chikungunya virus. Nat Rev Microbiol. 2010;8:491–500.
2. Huang YJ, Hsu WW, Higgs S, Vanlandingham DL. Temperature Tolerance and Inactivation of Chikungunya Virus. Vector Borne Zoonotic Dis. 2015;15:674–7.
3. Diallo M, Thonnon J, Lamizana-M T, Fontenille D. Vectors of Chikungunya virus in Senegal: current data and transmission cycles. Am J Trop Med Hyg. 1999;60:281–6.
4. Volk Sara M, Chen R, Tsetsarkin Konstantin A, Adams AP, Garcia Tzintzuni I, SallAmadou A, Nasar F, Schuh Amy J, Holmes Edward C, Higgs S, et al. Genome-scale phylogenetic analyses of chikungunya virus reveal independent emergences of recent epidemics and various evolutionary rates. J Virol. 2010;84:6497–504.
5. Zhang Y-N, Deng C-L, Li J-Q, Li N, Zhang Q-Y, Ye H-Q, Yuan Z-M, Zhang B. Infectious Chikungunya Virus (CHIKV) with a complete capsid deletion: a new approach for a CHIKV vaccine. J Virol. 2019;93:e00504-19.
6. Lin H-C, Chiao D-J, Lin C-C, Kuo S-C. Facile method for delivering chikungunya viral replicons into mosquitoes and mammalian cells. Sci Rep. 2021;11:12321.
7. Zhang Y-N, Deng C-L, Li J-Q, Li N, Zhang Q-Y, Ye H-Q, Yuan Z-M, Zhang B. Infectious Chikungunya Virus (CHIKV) with a complete capsid deletion: a new approach for a CHIKV vaccine. J Virol. 2019;93:1–16.
8. Renault P, Josseran L, Pierre V. Chikungunya-related fatality rates, mauritius, india, and reunion island. Emerg Infect Dis. 2008;14:1327.
9. Watson H, Tritsch SR, Encinales L, Cadena A, Cure C, Ramirez AP, Mendoza AR, Chang AY. Stiffness, pain, and joint counts in chronic chikungunya disease: relevance to disability and quality of life. Clin Rheumatol. 2020;39:1679–86.
10. Silva LA, Dermody TS. Chikungunya virus: epidemiology, replication, disease mechanisms, and prospective intervention strategies. J Clin Invest. 2017;127:737–49.
11. Arifuzzaman M, Collins N, Guo C-J, Artis D. Nutritional regulation of microbiota-derived metabolites: Implications for immunity and inflammation. Immunity. 2024;57:14–27.
12. Jiao L, Li H, Xu J, Yang M, Ma C, Li J, Zhao S, Wang H, Yang Y, Yu W, et al. The gastrointestinal tract is an alternative route for SARS-CoV-2 infection in a nonhuman primate model. Gastroenterology. 2021;160:1647–61.
13. Mizutani T, Ishizaka A, Koga M, Ikeuchi K, Saito M, Adachi E, Yamayoshi S, Iwatsuki-Horimoto K, Yasuhara A, Kiyono H, et al. Correlation analysis between gut microbiota alterations and the cytokine response in patients with coronavirus disease during hospitalization. Microbiol Spectr. 2022;10:e0168921.
14. Kamada N, Seo S-U, Chen GY, Núñez G. Role of the gut microbiota in immunity and inflammatory disease. Nat Rev Immunol. 2013;13:321–35.
15. Xue J, Ajuwon KM, Fang R. Mechanistic insight into the gut microbiome and its interaction with host immunity and inflammation. Anim Nutr. 2020;6:421–8.
16. Komatsu N, Takayanagi H. Mechanisms of joint destruction in rheumatoid arthritis — immune cell–fibroblast–bone interactions. Nat Rev Rheumatol. 2022;18:415–29.
17. Nakaya HI, Gardner J, Poo YS, Major L, Pulendran B, Suhrbier A. Gene profiling of Chikungunya virus arthritis in a mouse model reveals significant overlap with rheumatoid arthritis. Arthritis Rheum. 2012;64:3553–63.
18. Dedmon LE. The genetics of rheumatoid arthritis. Rheumatology. 2020;59:2661–70.
19. Häger J, Bang H, Hagen M, Frech M, Träger P, Sokolova M, Steffen U, Tascilar K, Sarter K, Schett G, et al. The role of dietary fiber in rheumatoid arthritis patients: a feasibility study. Nutrients. 2019;11:2392.
20. Zaiss MM, Joyce Wu H-J, Mauro D, Schett G, Ciccia F. The gut–joint axis in rheumatoid arthritis. Nat Rev Rheumatol. 2021;17:224–37.
21. Yan Z, Mingyue C, Liang Z, Luxu Y, Chaofang Z, Yuguo Z, Xue Z, Lei Z, Kang N, Jinxiang H. Hidden link in gut–joint axis: gut microbes promote rheumatoid arthritis at early stage by enhancing ascorbate degradation. Gut. 2022;71:1041.
22. Wang X, Ning Y, Li C, Gong Y, Huang R, Hu M, Poulet B, Xu K, Zhao G, Zhou R, et al. Alterations in the gut microbiota and metabolite profiles of patients with Kashin-Beck disease, an endemic osteoarthritis in China. Cell Death Dis. 2021;12:1015.
23. Messaoudi I, Vomaske J, Totonchy T, Kreklywich CN, Haberthur K, Springgay L, Brien JD, Diamond MS, DeFilippis VR, Streblow DN. Chikungunya virus infection results in higher and persistent viral replication in aged rhesus macaques due to defects in anti-viral immunity. PLoS Negl Trop Dis. 2013;7:e2343.
24. Khongwichit S, Chansaenroj J, Chirathaworn C, Poovorawan Y. Chikungunya virus infection: molecular biology, clinical characteristics, and epidemiology in Asian countries. J Biomed Sci. 2021;28:1–17.
25. Broeckel R, Haese N, Messaoudi I, Streblow DN. Nonhuman primate models of Chikungunya Virus Infection and Disease (CHIKV NHP Model). Pathogens. 2015;4:662–81.
26. Zhang R, Kim AS, Fox JM, Nair S, Basore K, Klimstra WB, Rimkunas R, Fong RH, Lin H, Poddar S, et al. Mxra8 is a receptor for multiple arthritogenic alphaviruses. Nature. 2018;557:570–4.
27. Meertens L, Hafirassou ML, Couderc T, Bonnet-Madin L, Kril V, Kümmerer BM, Labeau A, Brugier A, Simon-Loriere E, Burlaud-Gaillard J, et al. FHL1 is a major host factor for chikungunya virus infection. Nature. 2019;574:259–63.
28. Shalon D, Culver RN, Grembi JA, Folz J, Treit PV, Shi H, Rosenberger FA, Dethlefsen L, Meng X, Yaffe E, et al. Profiling the human intestinal environment under physiological conditions. Nature. 2023;617:581–91.
29. Negi S, Das DK, Pahari S, Nadeem S, Agrewala JN. Potential role of gut microbiota in induction and regulation of innate immune memory. Front Immunol. 2019;10:2441.
30. Iljazovic A, Roy U, Gálvez EJC, Lesker TR, Zhao B, Gronow A, Amend L, Will SE, Hofmann JD, Pils MC, et al. Perturbation of the gut microbiome by Prevotella spp. enhances host susceptibility to mucosal inflammation. Mucosal Immunol. 2021;14:113–24.
31. Larsen JM. The immune response to Prevotella bacteria in chronic inflammatory disease. Immunology. 2017;151:363–74.
32. Zhong X, Zhao Y, Huang L, Liu J, Wang K, Gao X, Zhao X, Wang X. Remodeling of the gut microbiome by Lactobacillus johnsonii alleviates the development of acute myocardial infarction. Front Microbiol. 2023;14:1140498.
33. Bae M, Cassilly CD, Liu X, Park S-M, Tusi BK, Chen X, Kwon J, Filipčík P, Bolze AS, Liu Z, et al. Akkermansia muciniphila phospholipid induces homeostatic immune responses. Nature. 2022;608:168–73.
34. Xu P, Shi Y, Liu P, Yang Y, Zhou C, Li G, Luo J, Zhang C, Cao H, Hu G, et al. 16S rRNA gene sequencing reveals an altered composition of the gut microbiota in chickens infected with a nephropathogenic infectious bronchitis virus. Sci Rep. 2020;10:3556.
35. Pianta A, Arvikar SL, Strle K, Drouin EE, Wang Q, Costello CE, Steere AC. Two rheumatoid arthritis–specific autoantigens correlate microbial immunity with autoimmune responses in joints. J Clin Invest. 2017;127:2946–56.
36. Alpizar-Rodriguez D, Lesker T, Gronow A, Gilbert B, Raemy E, Lamacchia C, Gabay C, Finckh A, Strowig T. Prevotella copri in individuals at risk for rheumatoid arthritis. Ann Rheum Dis. 2019;78:590–3.
37. Wen C, Zheng Z, Shao T, Liu L, Xie Z, Le Chatelier E, He Z, Zhong W, Fan Y, Zhang L, et al. Quantitative metagenomics reveals unique

gut microbiome biomarkers in ankylosing spondylitis. Genome Biol. 2017;18:142.
38. Scher JU, Sczesnak A, Longman R, Segata N, Ubeda C, Bielski CM, Rostron T, Cerundolo V, Pamer EG, Abramson SB, et al. Expansion of intestinal Prevotella copri correlates with enhanced susceptibility to arthritis. eLife. 2013;2:e01202.
39. Cua DJ, Tato CM. Innate IL-17-producing cells: the sentinels of the immune system. Nat Rev Immunol. 2010;10:479–89.
40. Toh M-L, Gonzales G, Koenders MI, Tournadre A, Boyle D, Lubberts E, Zhou Y, Firestein GS, van den Berg WB, Miossec P. Role of interleukin 17 in arthritis chronicity through survival of synoviocytes via regulation of synoviolin expression. PLoS One. 2010;5:e13416.
41. Chow A, Her Z, Ong EKS, Chen J-M, Dimatatac F, Kwek DJC, Barkham T, Yang H, Rénia L, Leo Y-S, et al. Persistent arthralgia induced by chikungunya virus infection is associated with interleukin-6 and granulocyte macrophage colony-stimulating factor. J Infect Dis. 2011;203:149–57.
42. Liu X, Poo Y, Alves J, Almeida R, Mostafavi H, Tang P, Bucala R, Teixeira M, Taylor A, Zaid A, et al. Interleukin-17 contributes to chikungunya virus-induced disease. mBio. 2022;13:e0028922.
43. Neupane B, Acharya D, Nazneen F, Gonzalez-Fernandez G, Flynt AS, Bai F. Interleukin-17A facilitates chikungunya virus infection by inhibiting IFN-α2 expression. Front Immunol. 2020;11:588382.
44. Round J, Lee S, Li J, Tran G, Jabri B, Chatila T, Mazmanian S. The toll-like receptor 2 pathway establishes colonization by a commensal of the human microbiota. Science. 2011;332:974–7.
45. Devriese S, Eeckhaut V, Geirnaert A, Van den Bossche L, Hindryckx P, van de Wiele T, Van Immerseel F, Ducatelle R, De Vos M, Laukens D. Reduced Mucosa-associated butyricicoccus activity in patients with ulcerative colitis correlates with aberrant claudin-1 expression. J Crohn's Colitis. 2017;11:229–36.
46. Konikoff T, Gophna U. Oscillospira: a central, enigmatic component of the human gut microbiota. Trendds Microbiol. 2016;24:523–4.
47. Odenyo AA, Mackie RI, Stahl DA, White BA. The use of 16S rRNA-targeted oligonucleotide probes to study competition between ruminal fibrolytic bacteria: development of probes for Ruminococcus species and evidence for bacteriocin production. Appl Environ Microbiol. 1994;60:3688–96.
48. Chaput N, Lepage P, Coutzac C, Soularue E, Le Roux K, Monot C, Boselli L, Routier E, Cassard L, Collins M, et al. Baseline gut microbiota predicts clinical response and colitis in metastatic melanoma patients treated with ipilimumab. Ann Oncol. 2017;28:1368–79.
49. Jama HA, Beale A, Shihata WA, Marques FZ. The effect of diet on hypertensive pathology: is there a link via gut microbiota-driven immunometabolism? Cardiovasc Res. 2019;115:1435–47.
50. Bouhaddou M, Memon D, Meyer B, White KM, Rezelj VV, Correa Marrero M, Polacco BJ, Melnyk JE, Ulferts S, Kaake RM, et al. The global phosphorylation landscape of SARS-CoV-2 infection. Cell. 2020;182:685-712.e619.
51. Ikeda M, Gunji Y, Sonoda H, Oshikawa S, Shimono M, Horie A, Ito K, Yamasaki S. Inhibitory effect of tyrphostin 47 on Shiga toxin-induced cell death. Eur J Pharmacol. 2006;546:36–9.
52. Sun L, Cai J, Gonzalez FJ. The role of farnesoid X receptor in metabolic diseases, and gastrointestinal and liver cancer. Nat Rev Gastroenterol Hepatol. 2021;18:335–47.
53. Liu F, Yao Y, Wang Q, Zhang F, Wang M, Zhu C, Lin C. Nigakinone alleviates DSS-induced experimental colitis via regulating bile acid profile and FXR/NLRP3 signaling pathways. Phytother Res. 2023;37:15–34.
54. Atarashi K, Tanoue T, Shima T, Imaoka A, Kuwahara T, Momose Y, Cheng G, Yamasaki S, Saito T, Ohba Y, et al. Induction of colonic regulatory T cells by indigenous clostridium species. Science. 2011;331:337–41.
55. Liu A, Zhang M, Wu Y, Zhang C, Zhang Q, Su X, Zhu X, Shi W, Liu J, Zhang Y, et al. ASPS exhibits anti-rheumatic effects by reprogramming gut microbiota and increasing serum γ-glutamylcysteine level. Adv Sci. 2023;10:2205645.
56. Hongyu C, Junbin W, Kaiyun D, Jingwen X, Yun Y, Cong T, Yanan Z, Wenhai Y, Haixuan W, Qing H, et al. Gastrointestinal microbiota and metabolites possibly contribute to distinct pathogenicity of SARS-CoV-2 proto or its variants in rhesus monkeys. Gut Microbes. 2024;16(1):2334970.
57. Hong Z, Yibin Z, Ziwen L, Yongmei P, Wenyu P, Liangqin T, Jinglin W, Qiyong L, Penghua W, Gong C. A volatile from the skin microbiota of flavivirus-infected hosts promotes mosquito attractiveness. Cell. 2022;185(14):2510-2522.e2516.
58. Zaid A, Gérardin P, Taylor A, Mostafavi H, Malvy D, Mahalingam S. Review: chikungunya arthritis: implications of acute and chronic inflammation mechanisms on disease management. Arthritis Rheumatol. 2018;70:484–95.

Publisher's Note